electronics

MDPI

Article

A Wirelessly-Powered Body-Coupled Data Transmission with Multi-Stage and Multi-Source Rectifier

Byeongseol Kim and Joonsung Bae *

Department of Electrical and Electronic Engineering, Kangwon National University, Chuncheon 24391, Republic of Korea; kimbs@kangwon.ac.kr
* Correspondence: baej@kangwon.ac.kr

Abstract: This paper demonstrates body-coupled (BC) data transmission and multi-source power delivery systems for neural interface applications. The implanted data transmitter and power receiver utilize an electrode interface rather than an antenna or coil interface for battery-free wireless transmission, enabling the external data receiver and power transmitter with patch electrodes to be placed away from the implant without requiring precise alignment, which is a critical issue in the conventional communication modalities of inductive coupling. Significantly, the implanted power receiver produces the supply voltage using ambient body-coupled 50/60 Hz signals from the Mains, on top of the 40.68 MHz wireless power source from the external power transmitter, to increase the recovered power level and the voltage conversion efficiency (VCE). The body-coupled wireless systems for implanted and external devices are implemented with integrated circuits (ICs) fabricated in a 180 nm CMOS process. When 650 mVpp AC voltage is applied to the implanted device, the power receiver recovers up to 780 µW with ambient (60 Hz signals) BC energy harvesting, achieving 93% VCE, while 600 µW is recovered without ambient (60 Hz signals) signal. The recovered power supplies the regulated voltage to the direct-digital signaling transceiver, which consumes 460 µW with an uplink data rate of 10 Mbps and a downlink data rate of 200 kbps, corresponding to an energy efficiency of 46 pJ/b.

Keywords: body-coupled (BC); wireless power; BC energy harvesting; ambient; BC data transceiver

Citation: Kim, B.; Bae, J. A Wirelessly-Powered Body-Coupled Data Transmission with Multi-Stage and Multi-Source Rectifier. *Electronics* **2023**, *12*, 2181. https://doi.org/10.3390/electronics12102181

Academic Editors: Gaetano Palumbo, Andrea Ballo and Orazio Aiello

Received: 13 April 2023
Revised: 3 May 2023
Accepted: 9 May 2023
Published: 10 May 2023

1. Introduction

A miniaturized neural interface that records and stimulates signals generated by the nervous system is an emerging treatment method to alleviate or treat symptoms without drugs and associated side effects [1,2]. The ultimate goal of neural interface research is to create links between the nervous system and the outside world to either treat or assist people with sensory, motor, or other disabilities of neural function. Fully implantable devices require wireless communication with devices outside the body. However, existing systems require physical connections to external hardware for power and data transfer. Therefore, most existing systems use a head-mounted device with a neural recording probe [3–5]. These systems interfere with highly mobile body parts, and forces applied to the implant can cause tissue damage and infection, limiting the long-term use of the device.

Wireless neural recording implants are robust and durable. Figure 1a shows that neural implants have recently been used using various wireless technologies. Existing wireless neural interfaces using radio frequency (RF) communication consume massive power to drive low-impedance antennas and generate enormous propagation loss through the tissues [6–8]. Another inductive link method [9] has a short transmission distance (11 mm) with sensitive alignment issues between coils of a large size of 10 mm × 10 mm in both TX and RX. Ultrasound is more robust to transceiver alignment than inductive link [10]. However, it has cranial absorption and limited data rate due to the tissue's low carrier frequency and frequency-dependent attenuation. The near-infrared method achieves a

small volume with micro LEDs [11]. However, propagation losses owing to scattering and alignment issues require surgical sub-cranial repeaters. A significant challenge for fully implantable wireless neural interfaces is minimizing the device's size for long-term compatibility and minimal tissue damage, so these conventional wireless neural interfaces have been reduced to the requirement of bulky components (such as coils, LEDs, and diodes), due to its high cost and size. In addition to the form factor, the biocompatibility requirements must also be addressed.

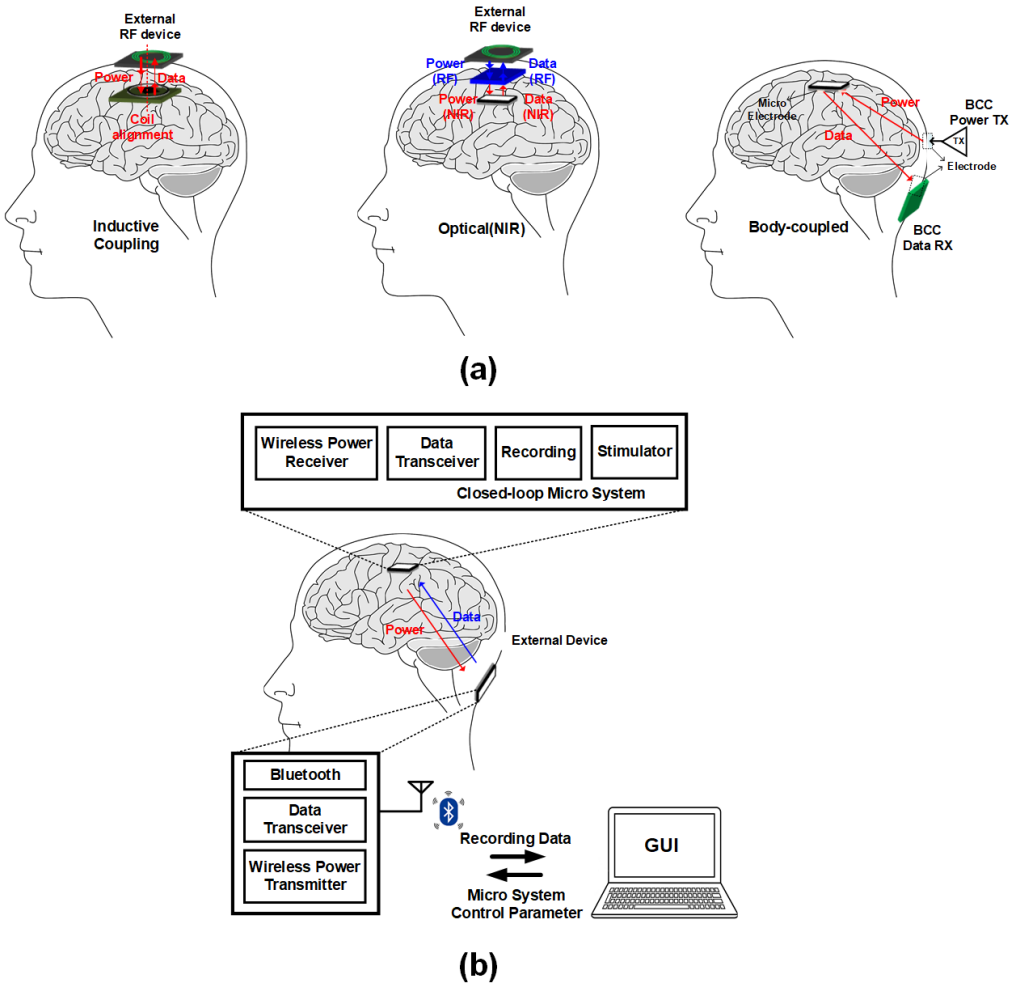

Figure 1. (**a**) Prior wireless neural implant systems and (**b**) Proposed system block diagram with BC power/data transmission.

This study presents the design, implementation, and verification of a wireless data transmitter structure driven by a wireless power receiver using a body-coupled (BC) modality (the rightmost of Figure 1a) [12–14]. The BC transmission, which has far less propagation loss in tissues than conventional RF methods, uses the body as a transmission channel. As the BC method uses the body's conductivity, only small and bio-compatible electrodes are required for interfacing with the human body and implanted and external devices. Thus, a small form factor can be achieved without the dedicated design of the antenna, coil, and transducer. Furthermore, precise alignment between devices is not required since a conductive signal path exists between implanted and external devices through the ionic cells in the body, which entails the increase of usability by locating the external device out of the head as a wireless repeater to interface with the smartphone or laptop via Bluetooth link (Figure 1b). The implant device is wirelessly powered while the data transceiver for uplink (from implant to external) and downlink (from external to implant) is optimized for energy efficiency and power consumption. The signal is passed

through the BC channel through conductive body tissue rather than the skull, creating a signal path between the electrodes attached to the implant and external devices. The small form factor system with microelectrode is implemented using a 180 nm CMOS process. Mainly, the power receiver employs the multi-stage and multi-source rectifier to increase the conversion efficiency of the power receiver, and the direct-digital signaling transceiver shows a 10 Mbps data rate, only consuming 460 μW.

The rest of this article is organized as follows. Section 2 discusses the characteristics of the BC channel for neural implants, including safety considerations of BC Transmission. Section 3 provides the neural implant architecture and implementation details related to BC power delivery and data transmission. Section 4 contains the measurement results. Finally, conclusions are presented in Section 5.

2. Channel Characteristics and Safety Considerations of BC Transmission

In order to use the body as a wireless channel, it is essential to figure out the channel response between TX and RX with safety considerations. Therefore BC channel characteristics and safety issues are addressed in this section.

2.1. Characteristics of Body-Coupled Channel

BC transmission for wearable devices has been adopted in several studies as an energy-efficient transmission method [15]. In the wearable device, the conductive layer of skin and tissue between electrodes forms a forward path, and the TX/RX ground forms a return path through capacitive coupling with the earth ground. The implant system forms a forward path similar to a wearable device. However, since the implant system is placed inside the body, there is no direct capacitive path between the body and the earth's ground. Therefore, it is essential to note the difference in signal path formation between the wearable and the implant. This section describes BC channel response from implant to external as well as from external to implant devices.

The characteristics of the body-coupled channel are investigated to figure out the path loss and the optimal frequency band, especially for the communication between implanted and external devices for power and data transmission. Figure 2 shows the in vitro measurements setup using the pork channel, the 'pork arm shoulder' part, with an area of 25 cm × 15 cm and a thickness of 1.5 cm. The battery-powered frequency synthesizer board, controlled from 100 kHz to 300 MHz, is fully implanted with the 0.43 mm^2 copper micro-electrode interface inside pork. The external battery-powered oscilloscope measures the received signal voltage from the implanted frequency synthesizer to obtain the channel gain and the frequency response with the differential Ag/AgCl electrodes with a diameter of 1 cm. The implanted device is located at a depth of 5 cm, and the surface distance is set to 5 cm and 10 cm. Figure 2b shows the measured frequency response when the surface distance is 5 cm and 10 cm. The 20~80 MHz frequency band shows the optimal channel loss with the relatively flat gain of −23 dB at 5 cm and −25 dB at 10 cm surface distance, which shows the high feasibility of the usage of the channel as a high bandwidth wireless data and high efficient wireless power transmission medium.

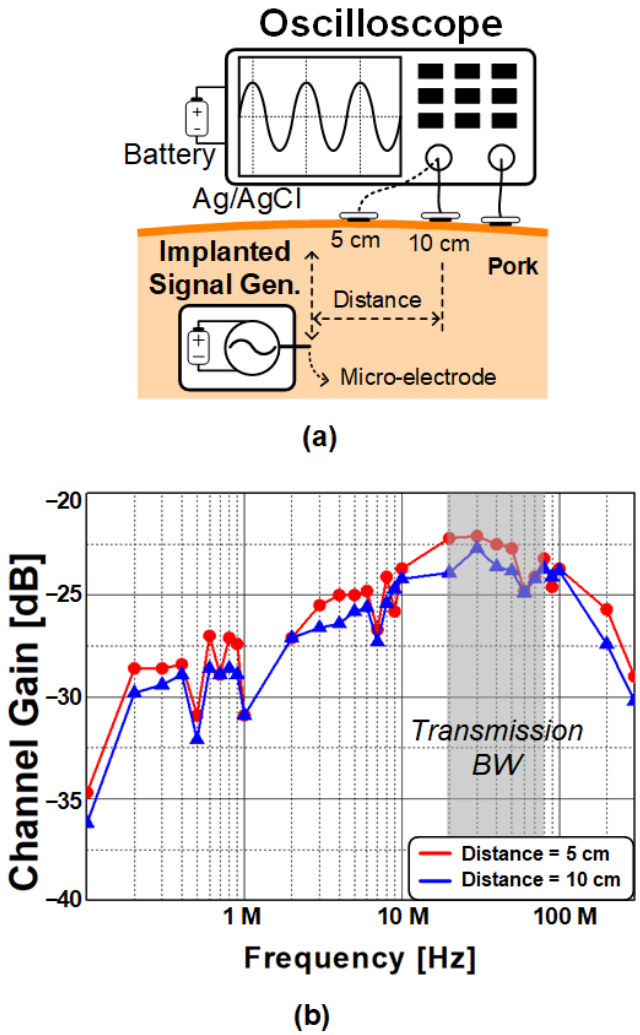

Figure 2. BC channel characteristics (uplink): (**a**) in vitro measurement setup and (**b**) frequency response.

While Figure 2 focuses on the channel gain for the data transmission path (uplink) from the implant to the external, Figure 3 describes the channel gain for the data transmission path (downlink) from the external to the implant with in-vitro experiment setup. As shown in Figure 3a, a microelectrode is inserted into the pork, and a signal is applied from the signal generator to the Ag/AgCl electrode connected to the skin. The pork channel, the 'pork arm shoulder' part, is utilized with an area of 25 cm × 15 cm and a thickness of 10 cm. The signal frequency from the signal generator is set to 40 MHz. Since it is challenging to monitor the received signal strength inside the body using an external device, indirect measurement was carried out after separating the ground between the external and implant devices. Channel gain was calculated utilizing a transfer function based on the input amplitude versus the output DC voltage from the WPR (Wireless Power Receiver) rectifier. A battery-powered digital multimeter was used to obtain the downlink channel gain. The measured results are shown in Figure 3b. The channel gain was measured with respect to the horizontal distance between the two electrodes with different insertion depths. The uplink path and downlink channel gains show less than −30 dB, even at a horizontal distance of 15 cm and an insertion depth of 8 cm. Also, the channel gain difference between the uplink and downlink was less than 0.5 dB at all distances, which means that the channel characteristics of the uplink and downlink are almost symmetrical.

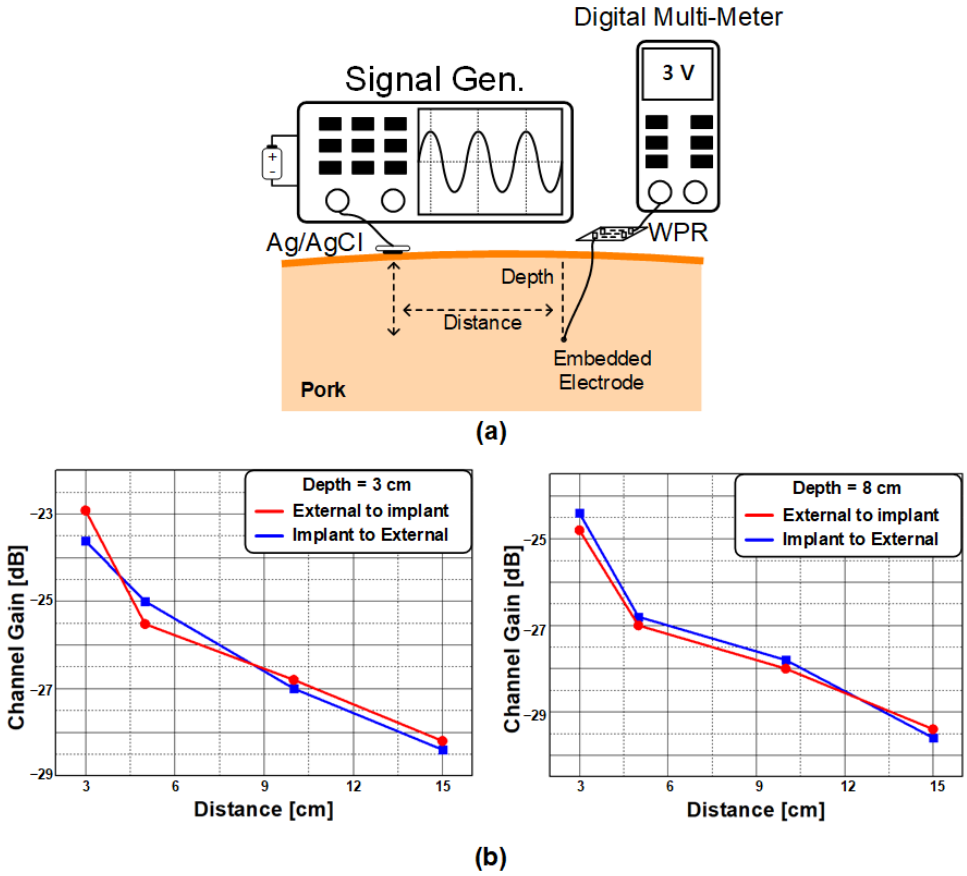

Figure 3. BC channel characteristics (downlink): (**a**) in vitro measurement setup and (**b**) measured channel gain versus the distance between the two electrodes.

2.2. Safety Considerations for BC Transmission

The body channel is a promising alternative to wireless communication for low-power operation via body communication and has been demonstrated as a body-coupled transmission medium. In recent years, body communications have emerged as a power-efficient alternative to traditional wireless communications. The method used in this paper transmits a signal by forming an electric field induced by an electrode. Small electrodes are used, and the conductive layer of the skin-body tissue between the electrodes forms a forward signal path. The parasitic capacitance component between the ground of TX/RX and the earth ground forms a return signal path. Accordingly, a closed loop is formed, enabling near-field voltage signal transmission. Regarding the safety of the proposed transmission method, the referenced regulation is the ICNIRP [International Commission on Non-Ionizing Radiation Protection (ICNIRP), "ICNIRP Guidelines for Limiting Exposure to Electromagnetic Fields (100 kHz to 300 GHz)," Health Phys., vol. 118, no. 5, pp. 483–524, March 2020 guideline]. ICNIRP has proposed guidelines for the maximum electric field, contact current, and SAR (Specific Absorption Rate) exposure. Within the frequency range of several tens of MHZ bands used in the proposed system, the main limiting quantities are contact current and SAR exposure. According to the published ICNIRP guideline, the maximum restrictions of the current density and the SAR for the frequency range are given as follows; contact current <20 mArms, and localized SAR (head) <2 W/kg.

The ICNIRP does not provide strict limits for contact currents and instead provides 'guidance' to assist those responsible for transmitting high-power radio-frequency fields to evaluate potential risks. Within the 100 kHz–110 MHz range, the ICNIRP considers that the lowest threshold would have been approximately 20 mArms for adults. The impedance through which the current flows is essential to calculate the current delivered and absorbed by the body. According to [12], the most critical factor determining the impedance when

applied to the proposed system is the capacitance between the implant system inserted into the body and the tissue. The capacitance determined by the contact area between the ground of the implant system and the tissue is less than 1 pF based on 4 mm^2 [12]. This is done in series with the impedance of the tissue and the capacitive coupling capacitance between the body and the earth's ground. If you estimate the impedance generated by the return path by referring to [12], it is more significant than 20 kΩ in the case of the frequency band used in the proposed system. So even when using a significant signal (=10 Vpp) from an external device, the maximum current will be ~500 μApp. This is well below the safety limit of 20 mArms proposed by the ICNIRP guidelines.

Regarding exposure to SAR, the biological and health effects established in the frequency band used by this system (>10 MHz) are comparable to the response to an increase in body temperature of 1 °C or more. This level of temperature rise is the result of exposure of an adult to a SAR of approximately 4 W/kg for approximately 30 min under a typical environment. The abovementioned contact current limitations are generally based on current magnitudes that will limit SAR in regions of small conductive cross section to less than the fundamental SAR restriction of the standard. Therefore, as the contact current of the proposed system is much smaller than the safety limits suggested by the ICNIRP explained earlier, it can be inferred that the proposed system also satisfies the restriction in terms of SAR exposures. In addition, since the proposed implantable system consumes only 460 μW, the energy absorbed by body tissues can be expected to be well below the ICNIRP SAR limit of 2 W/kg. In conclusion, the proposed system satisfies the ICNIRP requirements.

3. System Implementation

Figure 4 shows an overall block diagram of the proposed wireless-powered neural interface system. The external power transmitter sends a wireless power signal at 40.68 MHz, while the external data transmitter sends downlink data at a data rate of 200 kbps. The implanted device recovers the wireless power to the regulated DC voltage with a wireless receiver, and the 10 Mbps uplink transmitter sends high throughput data to the external device. Since the frequency spectrum of the data is limited to under 5 MHz, and the power signal is located at 40.68 MHz, the low pass filters in the data receiver separate the up/downlink signals from the narrowband wireless power signal. Meanwhile, the ISM band of 40.68 MHz is optimal for the power signal since it shows a significant signal transmission gain, as shown in Figure 2, as well as given the frequency spectrum of the data link, the lower frequency of the ISM band (13.56 MHz and 27.12 MHz) can corrupt the uplink data signal, which impedes the simultaneous operation of the data and power transmission. The multi-source rectifier makes use of the ambient 50/60 Hz signals, which are capacitively coupled to the body for enlarging the harvested power. The wireless receiver and data transceiver is implemented with the ICs to minimize the form factor of the implanted device in the proposed system.

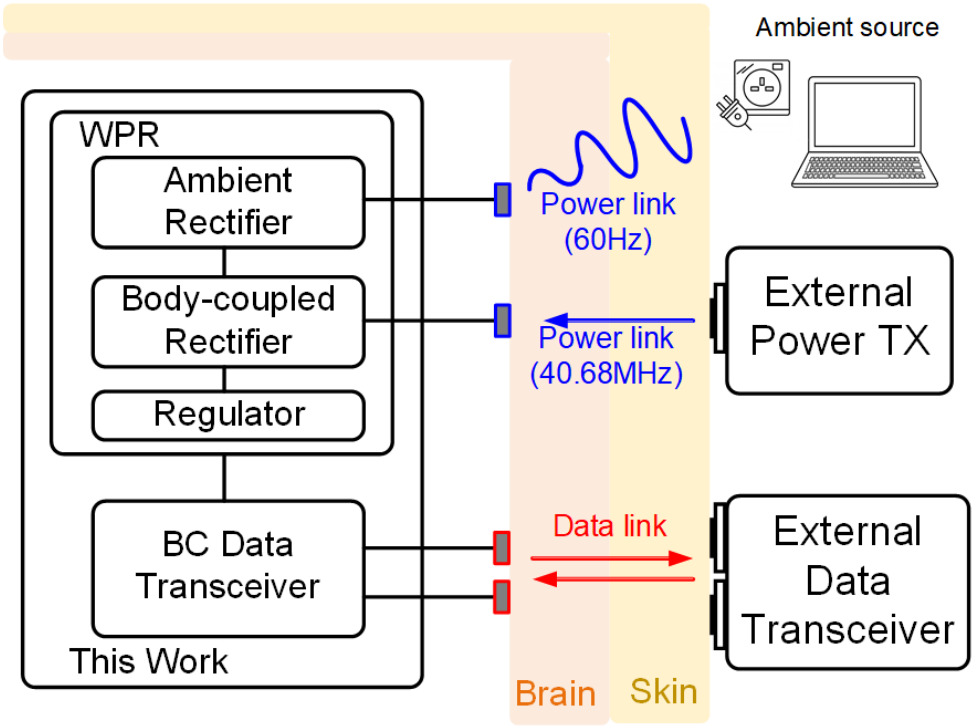

Figure 4. Overall block diagram of the proposed wirelessly-powered body channel communication system.

3.1. Wireless Power Receiver

Figure 5 shows the block diagram of the BC wireless power receiver, which consists of the multi-source step-up rectifier (MSR), bandgap reference (BGR), and low dropout regulator (LDO). The MSR is composed of the BC multi-stage rectifier and the ambient rectifier. On top of the DC voltage generated by the ambient rectifier using 50/60 Hz signals flowing through the surrounding environment and the body [15], the nine-stage cross-coupled rectifiers supplement the additional rectified voltage using the 40.68 MHz signal from the external power transmitter. The rectifier unit consists of 2 NMOSs and 2 PMOSs, which are cross-connected to each other. When a differential input signal is applied to VINAP and VINAN, assuming VINAP is larger than VINAN, Mp1 and Mn2 are turned on, while Mp2 and Mn1 are turned off. The gate-source voltages of the Mp1 and Mn2 are as enhanced as the level of twice the amplitude of the differential input. As a result, twice the input voltage amplitude is passed from the input source to the output, V_{out1}. On the other hand, alternately, when VINAN is larger than VINAP, Mp2 and Mn1 are turned on firmly and act as a full-wave rectifier to make the DC voltage of V_{out1}. In the case of an ambient rectifier, the voltage of V_{out1} is created based on the ground of the rectifier. The following BC multi-stage rectifier unit generates the DC voltage, V_{out2}, with the same cross-coupled rectifier units based on the V_{out1} level. With the multi-stages of the BC rectifier, the DC voltages are boosted to the V_{RECT}. The input of the ambient rectifier and the BC multi-stage rectifier is AC-coupled to the electrodes with off-chip capacitors and on-chip 10 pF capacitors, respectively. Given that the amplitude of the input signal is less than 1 V, the cross-coupled differential rectifier scheme using the input voltage to dynamically bias the gate voltage is optimal in the conversion efficiency due to the increased forward conduction current and suppressed reverse leakage current with a simple implementation. Then the rectified voltage (VRECT) supplies the BGR and LDO to generate VDDL (1.5 V) and VDD (3 V) for the BC transceiver.

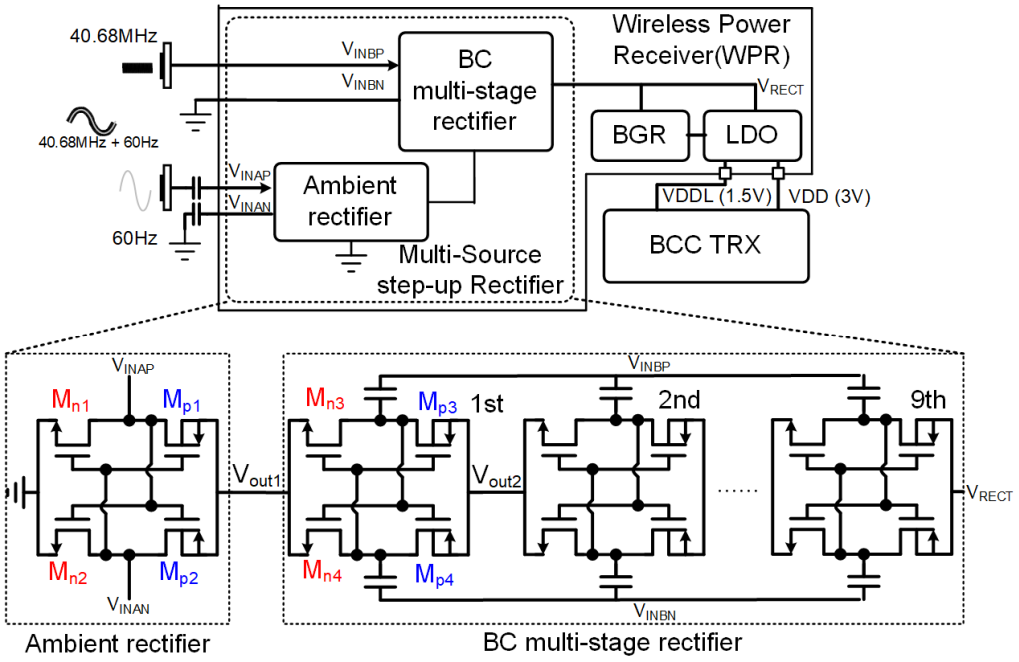

Figure 5. BC power RX block diagram and multi-stage rectifier schematic.

3.2. Body-Coupled (BC) Transmitter

Figure 6 shows the block diagram of the three-level clock-embedded signaling transmitter, which consists of the clock-embedded encoder and Tri-level power amplifier. It transmits three-level digital pulses with return-to-zero (RZ) signaling to embed the clock signal component, which can be extracted from the receiver side. To increase energy efficiency over the 10 Mbps data rate, most digital circuitry, including the clock-embedded encoder, is operated in the VDDL, while the Tri-level power amplifier drives the electrode with the level of VDD. The switching power amplifier is driven by the timing signals of Cont1, Cont2, Cont3, and Cont4 following the half-swing level shifter circuit to decrease the dynamic power consumption of the power amplifier to the capacitive load.

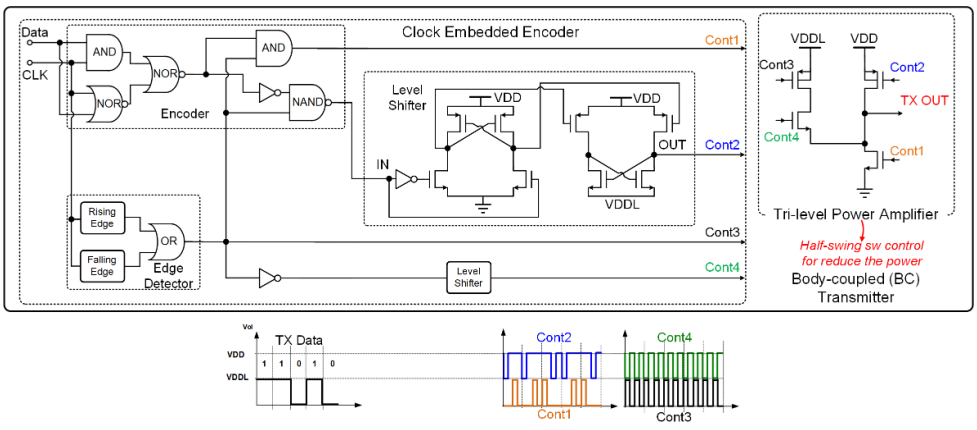

Figure 6. Block diagram of the BC data TX.

3.3. BC Receiver

Figure 7 shows the AC-coupled clocked comparator-based receiver (RX) block diagram with a squaring clock extraction scheme optimized for the tri-level RZ encoded TX signal. The LNA adopted a capacitive-coupled current-reuse input stage in the subthreshold region with a self-biasing scheme to achieve high transconductance. The Gilbert mixer squares the amplified signal through the LNA to extract a clock, followed by the clocked

StrongARM latch and Manchester decoder to recover the data and clock. Assuming the channel loss of 30 dB, the LNA is designed to have a gain of 26 dB and an input referred noise density of less than 13 nV/$\sqrt{}$Hz. The differential AC-coupled input structure is also utilized to eliminate any DC offset and low-frequency common-mode interference. A 40 MHz notch filter is adopted to eliminate the effects of the AC power signal of 40.68 MHz to be simultaneously operated with the wireless power recovery.

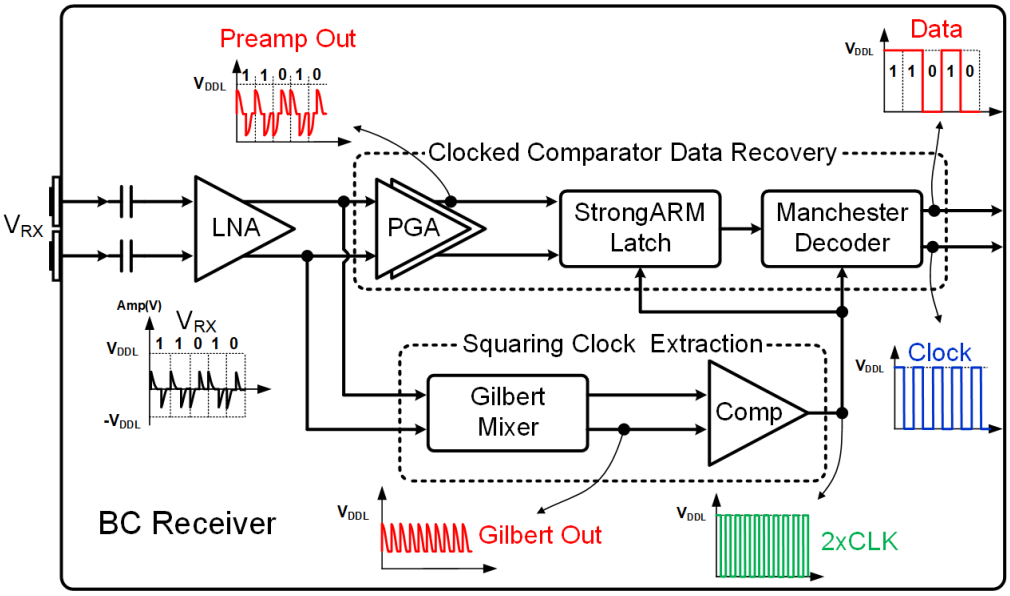

Figure 7. Block diagram of the BC data RX for clock and data recovery.

4. Measurement Results

Figure 8 shows the measurement results of the power receiver. A 40.68 MHz ISM band was used for the power link, and the signal generator's output voltage was varied between 300 mVpp and 650 mVpp. A signal generator (Keysight, 33600A Series) gave an input signal. Using the equipment, apply 40.68 MHz and 60 Hz signals to the test board using the coaxial SMA cable. The voltage generated by the WPR is applied across the output resistance (15 kΩ~1 MΩ), and a Digital Multi Meter (DMM, UNI-T, UT61D) equipment is used to monitor the voltage. Figure 8a shows the effects of the ambient rectifier with and without the ambient (60 Hz signals) signal when the amplitude of the 60 Hz signal is added with the amplitude from 500 mVpp to 1 Vpp under 15 kΩ load conditions. The efficiency improvement of the multi-source rectifier shows that the average output voltage of 0.51 V increases when the 1 Vpp ambient (60 Hz signals) signal is applied to the power receiver, corresponding to an enhancement of 10% VCE. Figure 8b shows the output power for the various load conditions. When the load is 15 kΩ, the wireless receiver can supply 753 μW when the input voltage amplitude is 650 mVpp. Therefore, the proposed wireless power receiver can efficiently supply enough power to the data transceiver inserted inside the body.

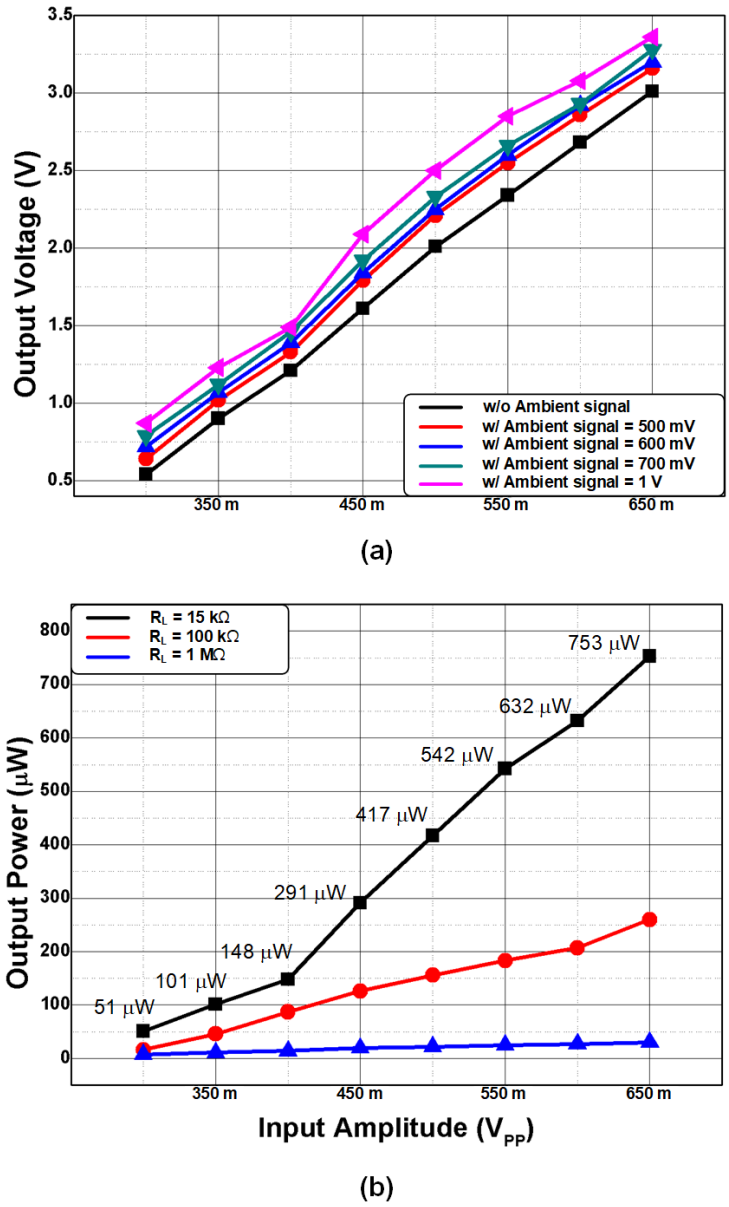

Figure 8. BC power RX measurement results: (**a**) input amplitude versus output voltage according to the amplitude of the ambient (60 Hz signals) signal and (**b**) input amplitude versus output power according to the load variation.

Figure 9 shows the uplink (a) and downlink (b) measurement setups (top) and the waveforms of the transmitted signal and recovered data and clock (bottom) of the BC transceiver, which is driven by the wireless power receiver simultaneously. First, for the channel, the pork arm shoulder was used, and the area was approximately 25 cm × 15 cm, and the thickness was 1.5 cm. Ag/AgCl electrodes were used for the electrodes outside the body, and microelectrodes with a size of 0.43 mm^2 were used for the electrodes assumed to be inside. In the case of uplink measurement, power is supplied externally using a signal generator (Keysight, 33600A Series). At the same time, data is transmitted to the channel using the power supplied by the WPR + BC TX test board. Afterward, the recovered data and clock signal were checked using an oscilloscope (Keysight, DSOX6004A) on the BC RX test board operated by battery. The distance between the transmitter electrode and the BC receiver electrode was 14 cm, and between the BC receiver electrode and the ambient (60 Hz signals) signal receiver electrode was 7 cm. The uplink communication was measured at 10 Mbps using a pork channel. The waveform showed the tri-level Tx waveform, recovered

clock, and data. The downlink communication was also evaluated using the pork channel at a data rate of 200 kbps.

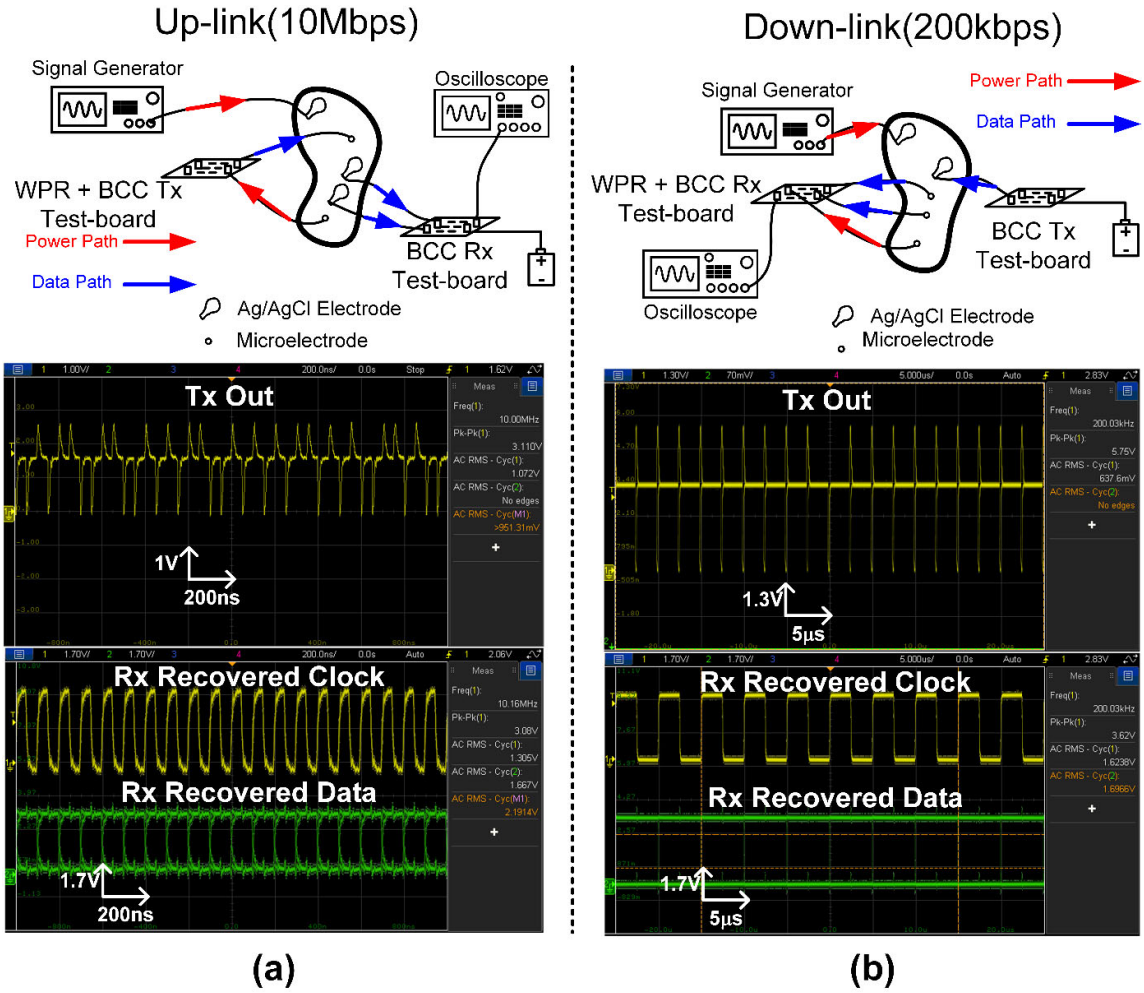

Figure 9. BC data TRX measurement results: (**a**) uplink path and (**b**) downlink path.

Figure 10 shows the chip microphotograph and performance summary. The IC is fabricated in a 180 nm CMOS process. The active areas of the power receiver, data transmitter, and data receiver are 1.1 mm × 0.5 mm, 1.4 mm × 0.3 mm, and 1 mm × 0.3 mm, respectively. Considering the performance summary, the wireless power receiver supplies up to 780 µW using 40.48 MHz and 60 Hz simultaneously, and the data TRX operates at 10 Mbps for uplink and 200 kbps for downlink. The energy efficiency is 46 pJ/b for TX and 470 pJ/b for RX. Table 1 shows a comparison with the results of previous studies showing that the proposed system demonstrates the battery-less wireless implanted transceiver with a multi-source wireless power receiver for neural interface applications.

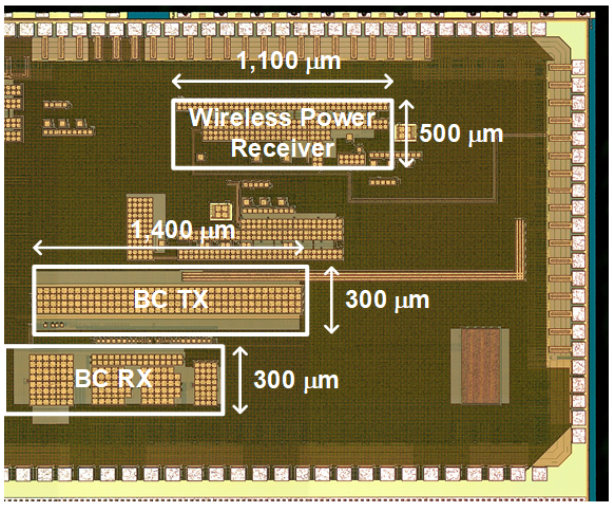

(a)

Wireless power receiver	
Frequency	40.68 MHz/60 Hz
Output Volt.	3 V/1.5 V
Output Power	780 μW @R_L = 15 kΩ

Data TRX	
Supply	3 V/1.5 V(Tx) 1.5 V(Rx)
Data rate (Mbps)	10(Up-link) 0.2(Down-link)
Power Consumption (μW)	460(Tx/10 Mbps) 95(Rx/200 kbps)
Energy/bit (J/b)	46 p(Tx/10 Mbps) 0.47 n(Rx/200 kbps)

(b)

Figure 10. (**a**) chip micrograph and (**b**) performance summary.

Table 1. Comparison to the state-of-the-art of a wirelessly-powered data transceiver.

	ASSCC [16]	ISSCC [17]	TBioCAS [6]	TBioCAS [15]	This Work
			Wireless Power Receiver		
Technology	180 nm CMOS	65 nm CMOS	0.35 μm CMOS	40 nm CMOS	180 nm CMOS
Power link	Inductive	Ultra-sound	Inductive	Body-coupled	Body-coupled
Rectifier Topology	Active-rectifier	Active-rectifier	Voltage-doubler	Cross-coupled	Cross-coupled
Frequency	6.78 MHz	0.95 MHz	13.56 MHz	40 MHz/60 Hz	40.68 MHz/60 Hz
Output volt. (V)	1/0.6/0.3	1	4/3.3/1.8	N.A.	3/1.5
Output power (μW)	N.A.	N.A.	N.A.	102.5	780
			Data TRX		
Supply (V)	1/0.3	1	N.A.		3/1.5
Data link	RF	Ultra-sound	RF/Inductive		Body-coupled
Modulation	OOK	OOK	OOK		Direct digital
Data rate (Mbps)	2	0.1/0.025	6.78/0.05		10/0.2
Power consumption (μW)	96	177	N.A.		460/95
Energy/bit (J/b)	48 p	1.77 n			46 p/470 p

5. Conclusions

This paper demonstrates body-coupled (BC) data transmission and multi-source power delivery systems for neural interface applications. The optimal frequency and the required specification of the transceiver design are obtained based on the in-vitro channel characteristics with the microelectrode and the implantable frequency synthesizer. The body-coupled wireless systems for implanted and external devices are implemented with integrated circuits (ICs) fabricated in a 180 nm CMOS process. Wireless power conversion efficiency is improved by using 40.68 MHz AC and 60 Hz ambient signals simultaneously, achieving up to 93% VCE. The low-power data transceiver with an electrode interface was optimized to be driven by a wireless receiver that supplies 3 and 1.5 V. A high speed of 10 Mbps uplink and low power of 200 kbps downlink is shown under the power consumption of 460 μW in the transmitter and 95 μW in the receiver. The corresponding energy efficiency values are 46 pJ/b and 0.47 nJ/b, respectively, demonstrating a promising potential for use in neural interface applications.

Author Contributions: Conceptualization, B.K. and J.B.; Methodology, B.K.; Writing—original draft, B.K.; Writing—review & editing, J.B. All authors have read and agreed to the published version of the manuscript.

Funding: This work was supported by Korea Institute for Advancement of Technology (KIAT) grant funded by the Korea Government (MOTIE) and This work is supported by the Technology Innovation Program under Grant 20012355 (Fully Implantable Closed Loop Brain to X for Voice Communication) funded By the Ministry of Trade, Industry & Energy (MOTIE).

Data Availability Statement: Not applicable.

Conflicts of Interest: The authors declare no conflict of interest.

References

1. Maharbiz, M.M.; Muller, R.; Alon, E.; Rabaey, J.M.; Carmena, J.M. Reliable next-generation cortical interfaces for chronic brain–machine interfaces and neuroscience. *Proc. IEEE* **2017**, *105*, 73–82. [CrossRef]
2. Muller, R.; Ghanbari, M.M.; Zhou, A. Miniaturized wireless neural interfaces: A tutorial. *IEEE Solid State Circuits Mag.* **2021**, *13*, 88–97. [CrossRef]
3. Lee, J.; Rhew, H.-G.; Kipke, D.R.; Flynn, M.P. A 64 channel programmable closed-loop neurostimulator with 8 channel neural amplifier and logarithmic ADC. *IEEE J. Solid State Circuits* **2010**, *45*, 1935–1945. [CrossRef]
4. Lopez, C.M.; Andrei, A.; Mitra, S.; Welkenhuysen, M.; Eberle, W.; Bartic, C.; Puers, R.; Yazicioglu, R.F.; Gielen, G.G.E. An implantable 455-active-electrode 52-channel CMOS neural probe. *IEEE J. Solid State Circuits* **2014**, *49*, 248–261. [CrossRef]
5. Van Daal, R.J.J.; Aydin, Ç.; Michon, F.; Aarts, A.A.A.; Kraft, M.; Kloosterman, F.; Haesler, S. Implantation of neuropixels probes for chronic recording of neuronal activity in freely behaving mice and rats. *Nat. Protoc.* **2021**, *16*, 3322–3347. [CrossRef] [PubMed]
6. Jia, Y.; Guler, U.; Lai, Y.; Gong, Y.; Weber, A.; Li, W.; Ghovanloo, M. A trimodal wireless implantable neural interface system-on-chip. *IEEE Trans. Biomed. Circuits Syst.* **2020**, *14*, 1207–1217. [CrossRef] [PubMed]
7. El Ansary, M.; Xu, J.; Filho, J.S.; Dutta, G.; Long, L.; Tejeiro, C.; Shoukry, A.; Tang, C.; Kilinc, E.; Joshi, J.; et al. Bidirectional peripheral nerve interface with 64 second-order opamp-less ΔΣ ADCs and fully integrated wireless power/data transmission. *IEEE J. Solid State Circuits* **2021**, *56*, 3247–3262. [CrossRef]
8. Xia, L.; Cheng, J.; Glover, N.E.; Chiang, P. 0.56 V, −20 dBm RF-Powered, Multi-Node Wireless Body Area Network System-on-a-Chip with Harvesting-Efficiency Tracking Loop. *IEEE J. Solid State Circuits* **2014**, *49*, 1345–1355. [CrossRef]
9. Li, W.; Duan, Y.; Rabaey, J.M. A 200 Mb/s inductively coupled wireless transcranial transceiver achieving 5e-11 BER and 1.5 pJ/b transmit energy efficiency. In Proceedings of the 2018 IEEE International Solid-State Circuits Conference (ISSCC), Digital Technology Papers, San Francisco, CA, USA, 11–15 February 2018; pp. 290–292.
10. Ghanbari, M.M.; Piech, D.K.; Shen, K.; Alamouti, S.F.; Yalcin, C.; Johnson, B.C.; Carmena, J.M.; Maharbiz, M.M.; Müller, R. 17.5 A 0.8 mm^3 Ultrasonic Implantable Wireless Neural Recording System with Linear AM Backscattering. In Proceedings of the 2019 IEEE International Solid-State Circuits Conference (ISSCC), San Francisco, CA, USA, 17–21 February 2019; pp. 284–286.
11. Lee, S.; Cortese, A.J.; Trexel, P.; Agger, E.R.; McEuen, P.L.; Molnar, A.C. A 330 μm × 90 μm opto-electronically integrated wireless system-on-chip for recording of neural activities. In Proceedings of the 2018 IEEE International Solid-State Circuits Conference (ISSCC), San Francisco, CA, USA, 11–15 February 2018; pp. 292–294.
12. Lee, C.; Kim, B.; Kim, J.; Lee, S.; Jeon, T.; Choi, W.; Yang, S.; Ahn, J.; Bae, J.; Chae, Y. A Miniaturized Wireless Neural Implant with Body-Coupled Power Delivery and Data Transmission. *IEEE J. Solid State Circuits* **2022**, *57*, 3212–3227. [CrossRef]
13. Yuk, B.; Kim, B.; Park, S.; Huh, Y.; Bae, J. An Implantable Body Channel Communication System with 3.7-pJ/b Reception and 34-pJ/b Transmission Efficiencies. *IEEE Solid-State Circuits Lett.* **2020**, *3*, 50–53. [CrossRef]
14. Kim, B.; Yuk, B.; Bae, J. A Wirelessly-Powered 10 Mbps 46-pJ/b Body Channel Communication System with 45% PCE Multi-Stage and Multi-Source Rectifier for Neural Interface Applications. In Proceedings of the 2021 IEEE Asian Solid-State Circuits Conference (A-SSCC), Busan, Republic of Korea, 7–10 November 2021; pp. 1–3.
15. Li, J.; Dong, Y.; Park, J.; Lin, L.; Tang, T.; Yoo, J. Body-Area Powering with Human Body-Coupled Power Transmission and Energy Harvesting ICs. *IEEE Trans. Biomed. Circuits Syst.* **2020**, *14*, 1263–1273. [CrossRef] [PubMed]
16. Huang, H.; Zhang, M.; Li, G.; Wang, Z. A 2Mbps sub-100 μW Crystal-less RF Transmitter with Energy Harvesting for Multi-Channel Neural Signal Acquisition. In Proceedings of the 2019 IEEE Asian Solid-State Circuits Conference (A-SSCC), Macau, China, 4–6 November 2019; pp. 157–160.
17. Chang, T.C.; Wang, M.L.; Charthad, J.; Weber, M.J.; Arbabian, A. 27.7 A 30.5 mm^3 fully packaged implantable device with duplex ultrasonic data and power links achieving 95kb/s with <10−4 BER at 8.5 cm depth. In Proceedings of the 2017 IEEE International Solid-State Circuits Conference (ISSCC), San Francisco, CA, USA, 5–9 February 2017; pp. 460–461.